Journal of Fish Diseases

# Morphopatology and gill recovery of Atlantic salmon during the parasitic detachment of Margaritifera margaritifera

| | |
|---|---|
| Journal: | *Journal of Fish Diseases* |
| Manuscript ID | JFD-2021-44 |
| Wiley - Manuscript type: | Research Article |
| Date Submitted by the Author: | 03-Feb-2021 |
| Complete List of Authors: | Castrillo, Pedro A.; Universidade de Santiago de Compostela<br>Varela-Dopico, Catuxa; Universidade de Santiago de Compostela<br>Bermúdez, Roberto; Universidade de Santiago de Compostela<br>Ondina, Paz; Universidade de Santiago de Compostela<br>Quiroga, Mª Isabel; Universidade de Santiago de Compostela |
| Keywords: | |
| Keywords: | gill healing, parasite detachment, Salmo salar, glochidiosis, Freshwater Pearl Mussel |
| | |

# Morphopatology and gill recovery of Atlantic salmon during the parasitic detachment of *Margaritifera margaritifera*

**Short running title:** Gill recovery after the parasite detachment

Castrillo, Pedro A.[1]; Varela-Dopico, Catuxa[2]; Bermúdez, Roberto[1,3]; Ondina, Paz[2]; Quiroga, María Isabel[1,3]

1. Department of Anatomy, Animal Production and Veterinary Clinical Sciences, Faculty of Veterinary, Universidade de Santiago de Compostela, Lugo, Spain.

2. Department of Zoology, Genetics and Physical Anthropology, Faculty of Veterinary, Universidade de Santiago de Compostela, Lugo, Spain.

3. Instituto de Acuicultura, Universidade de Santiago de Compostela, 15705, Santiago de Compostela, Spain.

ORCID: Pedro A. Castrillo: 0000-0001-5499-7190; Catuxa Varela-Dopico: 0000-0002-3513-1444; Roberto Bermúdez Pose: 0000-0003-4969-4122; Paz Ondina: 0000-0003-4392-9250; María Isabel Quiroga: 0000-0001-6832-7665

**Correspondence**

Roberto Bermúdez, Department of Anatomy, Animal Production and Veterinary Clinical Sciences, Faculty of Veterinary, Universidade de Santiago de Compostela, Campus Universitario s/n, 27002, Lugo, Spain. Email: roberto.bermudez@usc.es



**Acknowledgments**

The authors would like to thank the assistance of Dr. R. Mascato and R. Ocharan with the field work and the captivity procedures during this long-term experimental trial. Also, we warmly thanks S. Maceiras for the thorough histopathological technical assistance and Dr. A. M. de Azevedo, Dr. A. P. Losada and Dr. P. Ronza for the scientific advices. The conservation programme was cofunded by the "Fundación Biodiversidad" within the MarMaCul and MargaSalmo Projects and by the Xunta de Galicia within "Programa de Consolidación e Estructuración de Unidades de Investigación Competitivas" (ED4313 2019/24 and ED431D 2017/22) for the regional development for scientific network. P. A. Castrillo held a University Professorship Formation (FPU) grant from the Spanish Ministry of Education, Culture and Sport (FPU17/02004). We also acknowledge the support of the research collaboration agreement with the Consellería de Medio Ambiente, Territorio y Vivienda (Xunta de Galicia).

## Data availability statement

The data that support the findings of this study are available from the corresponding author upon reasonable request.

## Conflict of interest statement

The authors declare that they have no competing interests.


## Abstract

During the conservation aquaculture of the freshwater mussel *Margaritifera margaritifera*, fish health has become a concern due the need of mussel larvae (glochidia) to parasitize the salmonid gills and metamorphose into juveniles. However, there is lack of information about the impact on fish during the juvenile detachment and the subsequent gill healing. To evaluate the morphopathological changes and gill recovery after the parasitism of *M. margaritifera*, fifty-one Atlantic salmon fry (*Salmo salar*), infested with around 22 larvae/fish g, were necropsied during the synchronized detachment of the mussel juveniles, and gills were assessed by stereomicroscopy, and by light and scanning electron microscopy. Salmon showed no clinical signs during the trial and gills recovered their normal morphology almost completely in a short time, suggesting a minimal impact on fish health after glochidiosis. In this sense, the non-erosive droplet detachment and the goblet cell hyperplasia favored an effective gill remodeling mediated by apoptosis, polarization and cell shedding of the gill epithelia, providing insights to the defense, clearing and healing mechanisms of the gill. These morphopathological techniques could also be implemented to preserve fish welfare and to optimize the artificial breeding programmes of endangered freshwater mussels.





## Keywords

gill healing, Freshwater Pearl Mussel, fish pathology, parasite detachment, *Salmo salar*, glochidiosis

## 1 Introduction

Freshwater mussels are bivalves with extraordinary capacities of biofiltration and burrowing, thus, they provide significant ecosystem services and also indirectly protect many other species (Vaughn, 2017). Despite its importance, certain naiads as *Margaritifera margaritifera* (L., 1758) are categorized in the European Red List of IUCN as Critically Endangered due to the serious decline of the populations (Cuttelod, Seddon & Neubert, 2011). To protect the most affected populations, which lack natural recruitment (Lois, Ondina, Outeiro, Amaro & San Miguel, 2014), one emergency conservation strategy is to implement artificial breeding programmes (Gum, Lange & Geist, 2011).

The culturing techniques of freshwater mussels depend on the compulsory larval parasitic stage on Atlantic salmon (*Salmo salar* L.) and brown trout (*Salmo trutta* L.) fry, regarded as a mechanism of dispersal, nutrition and protection (Barnhart, Haag & Roston, 2008; Denic, Taeubert & Geist, 2015; Geist, 2010). In particular, the larva of *M. margaritifera* clamps and encysts into the salmonid gills for several months until it detaches in spring—once temperature rises over 15 ºC—as a free-living juvenile (Hruska, 1992; Taeubert, Gum & Geist, 2013). Accordingly, fish suffer a multifocal proliferative branchitis, which leads to a disease status known as glochidiosis, given by the name of the infesting larvae, the glochidium (Karna & Millemann, 1978).

This host-parasite interaction supposes a bottleneck for freshwater mussel aquaculture and a concern towards the welfare of the host fish. In an attempt to optimize the culturing efforts several studies had established certain recommended glochidial loads (Taeubert & Geist, 2013), based on the impact on fish survival, growth, respiration, metabolism, swimming capacity and fish behavior (Chowdhury, Marjomäki & Taskinen, 2019; Cunjak & McGladdery, 1991; Filipsson, Brijs, Näslund, Wengström, Adamsson *et al.*, 2017; Österling, Ferm & Piccolo, 2014; Preston, Keys & Roberts, 2007; Thomas, Taylor & Garcia de Leaniz, 2013). However, there is a lack of data about the pathogenesis of the disease, in which the morphopathological evaluation of the gill lesions remain overlooked, mostly focused on the premature rejection of unviable larvae, which is associated to an erosive branchitis during early stages of glochidiosis (Castrillo, Varela-Dopico, Ondina, Quiroga & Bermúdez, 2020). This contrast with the extensive knowledge of other gill ectoparasites which compromise the fish welfare in aquaculture, *e.g.*, *Neoparamoeba perurans* and *Ichthyophthirius multifiliis* (Powell, Leef, Roberts & Jones, 2008; Tumbol, Powell & Nowak, 2001). Lastly, gills are able to recover after removal of the inciting cause as chemicals or infectious agents (Daoust & Ferguson, 1986; Kudo & Kimura, 1983; Sales, Santos, Rizzo, Ribeiro, Santos *et al.*, 2017; Speare, Carvajal & Horney, 1999); nevertheless, very few studies

refer to the recovery of lesions after glochidiosis (Kaiser, 2005; Karna & Millemann, 1978; Scharsack, 1994; Treasurer & Turnbull, 2000).

Employing this artificial glochidiosis as a model of parasitic gill disease and recovery in Atlantic salmon, the purpose of this study was to perform a comprehensive morphopathological evaluation during the late stages of glochidiosis including the juvenile detachment and the subsequent gill healing process. Hence, this study may also provide insights to understand this complex host-parasite interaction and to preserve fish welfare during the rearing of these important and endangered freshwater mussels.

## 2 MATERIAL AND METHODS

### 2.1 Experimental gill infestation and selection of infested fish

Experimental fish came from an artificial glochidiosis trial performed in September 2015 (Castrillo *et al.*, 2020). Briefly, 1000 salmon fry were exposed by bath immersion to *M. margaritifera* glochidia (1,000 glochidia /fish gram) collected from gravid wild mussels. A group of non-exposed fish served as control group. At day 14 post-exposure (PE) an early detachment of inviable glochidia occurred and successfully infected fish could be only identified by means of light microscopy, due to the larval size at this stage (diameter of 70 µm).

After this early rejection, the remaining salmon were reared for six more months to allow the development of the encysted larvae and became macroscopically visible on the gill (diameter of 350 µm). Thus, after 202 days postexposure (PE), each exposed fish could be *in vivo* diagnosed as infested or non-infested by manual immobilization, abduction of the opercula and gill visualization. This diagnostic procedure was performed in less than four seconds. As a result, 51 out of 600 exposed fish were selected as infested (prevalence of 8.5%). The same exploratory procedure was performed on 51 non-exposed fish. Moreover, to ensure an optimal fish health status and confirm the absence of any other pathological processes prior the *in vivo* procedure, five exposed and non-exposed fish were necropsied and processed for histopathology.

### 2.3 Synchronization of juvenile detachment

Infested and control fish ($n$ = 51, mean weight 5.8 g and length 8.1 cm) were relocated into a recirculating system to synchronize the detachment of *M. margaritifera* juvenile mussels by exposing fish to high water temperatures for several weeks (Hruska, 1992). Thereby, the temperature was daily heated 1º up to 17ºC, and thereafter maintained constant until the end of the experiment (± 0.2; Supplementary table 1) by employing a temperature control system (Aquarium Controller Evolution, Aquatronica®) and a thermostat (Ako®). Moreover, water was

pretreated by mechanical filtration and ultraviolet irradiation, and the exchange rate was set at 2,000 L/h with a degree of recirculation of 98% (± 0.2). Water quality was periodically monitored in each tank by measuring ammonia, nitrite, and nitrate with a photometer (HI83203, HANNA instruments®), and pH and dissolved oxygen by a pH/dissolved oxygen meter (PD 650 meter, Oakton®) (Supplementary table 1). Both batches were fed with a commercial dry pellet (AquaPro, Skretting®) at about 0.5% body weight to minimize the input of ammonia into the system and the fish mortalities were daily checked.

The detached mussel juveniles were daily collected from the tank outlet by sieves with a mesh size of 150 µm. Later on, they were pipetted, counted under the stereomicroscope, and classified as viable or unviable for culturing based on the presence or absence of pedal and valve movements, respectively. Additionally, viable juveniles were photographed with a Leica® M125 stereomicroscope and a M170HD digital camera. Since the number of experimental fish was reduced due to the sampling procedure, mussel juveniles counts were standardized considering the number of remaining fish left in the tank in juveniles/fish.

### 2.4 Sampling procedure: determination of the opercular rate and necropsy

Eight infested and control fish were randomly sampled at day 203, 221, 225, 232 and 239 PE, focusing on the juvenile detachment. At 246 PE, the remaining eleven fish of each group were sampled to conclude the study. After hand-netting, fish were individually held into individual transparent buckets with 1 L of water, and the opercular movements were measured for 20 s twice (3 and 15 min after net capture) to calculate the mean opercular rate of each fish, expressed in opercular beats/min (OBM).

Afterwards, salmon were individually anesthetized and euthanized by overexposure to a solution of 200 mg/L of tricaine methanesulfonate (MS-222, Sigma-Aldrich®) buffered with 400 mg/L of sodium bicarbonate. Euthanasia was confirmed by sectioning the spinal cord. Weight (± 0.1 g), fork length (± 0.1 cm) and Fulton´s condition factor (100×weight (g)/length (cm)$^3$) were calculated and standard deviation expressed (±). Immediately, the whole animal was immersed in water in lateral decubitus, the operculum was abducted and the left holobranchs were stereomicrophotographed employing the previous equipment.

Subsequently, complete necropsy of animals was performed, and right holobranchs and other organs (skin, thymus, digestive tract, heart, kidney and spleen) were sampled and immediately fixed in Bouin's fixative for 18 hr. For scanning electron microscopy (SEM), a small portion of gill tissue was fixed first in 2.5% glutaraldehyde with 0.1 M cacodylate buffer (pH 7.3) and then in 1% osmium tetroxide. Left holobranchs were dissected out and examined to estimate the larval load of infested fish, standardized by fish weight (larvae/fish g) according to Marwaha, Aase,

Geist, Stoeckle, Kuehn *et al.* (2019). Lateral stereomicrophotographs of each left holobranch were obtained using the previous equipment to evaluate the larval distribution in the gill. Additional microphotographs were captured with a Leica® DM750 light microscope a ICC50HD digital camera to evaluate the encysted larvae and measure their length as previously described ($n$ = 80, ± 0.1 µm).

All procedures were carried out at the facilities of "Centro Ictiogénico de O Veral" (Xunta de Galicia) and followed the international (Directive 2010/63/EU, on the protection of animals used for scientific purposes), national (Law 6/2013 and RD 53/2013, on the protection of animals used for scientific experiments) and institutional regulations (USC Review Board).

### 2.5 Light and scanning electron microscopy (SEM)

After Bouin´s fixation, right holobranchs were decalcified for 6 h in a 10% ethylenediaminetetraacetic acid (EDTA) solution (Osteodec, Bio-optica®). Decalcified holobranchs and remaining organs were processed for histopathology by routine methods and sections (3 µm) from paraffin-embedded tissue were stained with hematoxylin and eosin (H&E). Gill tissue was additionally stained with periodic acid-Schiff (PAS) and Masson-Goldner trichrome. Slides were observed and photographed using an Olympus® BX51 light microscopy equipped with an DP72 or EP50 digital cameras. On the other hand, samples for SEM were dehydrated in ethanol solutions and routinely processed for examination under a JEOL JSM-6360LV scanning electron microscope.

### 2.6. Statistical analysis

The quantitative variables, body condition and opercular rate, were statistically compared between groups employing the Wilcoxon-Mann-Whitney U test. The strength of the relationships between body condition and opercular rate with the parasitic loads were calculated during the first three samplings (day 203, 221, 225 PE) employing the Spearman´s Correlation Coefficient. In addition, the daily length of the recently detached juveniles was included into the study. The significance level was 95% in all cases ($p$-value < .05). All the numeric data were analyzed by RStudio software (R Core Team, 2019).

## 3 RESULTS

During the late glochidiosis, no mortalities were observed and fish displayed a mean body condition of 0.98 ± 0.08 and a mean opercular rate after hand-netting of 135 ± 13, with similar values between the infested and the control group throughout most of the samplings (Figure S1). Moreover, the juvenile detachment was successfully synchronized between day 203 and 238 PE,

yielding a total of 13,891 juveniles of *M. margaritifera*. During this period, the detachment displayed a left-skewed distribution with a peak of 38 detached juveniles/fish at day 226 PE (Figure 1a). Based on the curve of this detachment, three stages could be established to better describe the evolution of the juvenile detachment in relation with the fish parasitosis and the histopathological changes (Figure 1a and b): the rising detachment stage (day 203–226 PE), the declining detachment stage (day 227–238 PE) and the post-detachment stage (day 239–246 PE).

### 3.1. The rising detachment stage (day 203–226 PE)

At the necropsy, 96% of fish were infested (Figure 1b) and harbored a median parasitic load of 22.4 ± 47.4 larvae/fish g, in which highly infested fish in the upper quartile showed a mean of 102 larvae/fish g; meanwhile, the remaining fish below the upper quartile displayed a mean of 12.6 larvae/fish g (Figure 1c). No significant relationships were detected in the correlation analysis between the parasitic load and the body condition nor the opercular rate after hand-netting (Figure 1c).

By naked eye visualization of infested fish, abundant, well-delimited, punctiform nodules were observed in the branchial tissue (Figure 2a). By stereomicroscopy, the immersed gills revealed a high number of ivory bean-shaped parasitic nodules located on the four holobranchs (Figure 2b), mostly at the trailing edges of the filaments (Figure 2c). Fish with less than 58 larvae/fish g exhibited a distinctive distribution of the larvae, clustered in bunches, which tended to gather at the dorsal and ventral regions of each holobranch (Figure 2d).

By light microscopy at low magnifications, the parasitic clusters were composed of several large and protruding nodules. Each nodule corresponded with a cyst of *M. margaritifera* larva, surrounded by a well-localized epithelial response in which adjacent lamellae, and sometimes the adjacent filaments, were fused obliterating the gill exchange surface (Figure 2e and f). Often, fused lamellae became elongated up to twice their length (Figure 2f and 3c). The parasitic cysts were completely covered by an intense epithelial hyperplasia and hypertrophy, the latter characterized by the high number of epithelial cells with large swollen cytoplasm, ovoid nucleus and small nucleoli (Figure 2g). Mitotic figures were frequently detected all over the cyst, although they were more abundant basally at the interlamellar epithelium of the parasitized regions (Figure 2f). The epithelial cells closest to the bivalve periostracum concentrically arranged and became thinner, elongated and intensely eosinophilic with H&E, being also PAS-positive (Figure 2g). Associated to the parasitosis, a lymphocytic inflammatory infiltrate was interspersed between the hyperplastic epithelium (Figure 2g). Moreover, a mixed inflammatory cell population, composed by macrophages and polymorphonuclear cells, was identified at the deeper layers of the filaments and related to the interlamellar system, particularly underneath the basal membrane of small

ladder-like vessels (Figure 2h) and marginated over the endothelium of elongated sinus (Figure 2i).

No other lesions were recorded in other sampled organs from infested fish. On the other hand, control fish exhibited unfused lamellae, intraepithelial lymphocytes at the trailing edge of the filaments and scarce inflammatory cells associated to the interlamellar system (Figure 2j).

Some parasitic nodules bulged to a high extent on the gill surface (Figure 3a), molding the contiguous filaments observed as focal areas with concave shape (Figure 2e). Furthermore, fresh microscopy highlighted the undisturbed arterioles underneath the parasitic cyst (Figure 3b) and exceptionally devious arterioles were related to the encysted larvae at the filamental tips (Figure 3c). In these cases, the growth plaque of the filament was also deviated (Figure 3d) and the cartilage ray was thickened due to an irregular disposition of hyperplastic chondrocytes, observed by histology (Figure 3e). Under SEM, the nodular surface was covered by flattened and polygonal epithelial cells, overlaid by well-defined microridges (Figure 3f). However, at the most protruding regions, a localized epithelial degeneration occurred, characterized by the presence of faint microridges and cell boundaries (Inset, Figure 3f). Histologically, the contact area between these larger nodules and the filaments became reduced (50–100 μm width) creating a pedunculated, teardrop shaped structure supported by the hyperplastic epithelium of fused lamellae (Figure 3g). Occasionally, the encysted parasites were barely linked to the gill tissue by a very constricted and pinched-off peduncle which showed a superficial goblet cell hyperplasia (Figure 3h). Moreover, at deeper layers, the hyperplastic tissue was accompanied by moderate epithelial apoptosis, observed by pyknosis, cell shrinkage and the presence of apoptotic bodies (Figure 3h). Based on the overall morphopathological features described, larvae sloughed from the gill by a *droplet detachment* mechanism, illustrated in Figure 3i and simplified in three sequential steps: 1. protrusion over the surrounding limits, 2. pinch-off by reduction of the contact area between the gill and 3. detachment of the larvae without tissue disruption.

The encysted larvae displayed a thin and refringent periostracum under fresh microscopy, which allowed to discern the valves completely closed, the valve rims facing each other and the discernible mantle within the internal pallial and extrapallial cavities (Figure 3j). Once detached from the gills, the recently sloughed and viable juveniles exhibited mobile valves and a protractile foot protruding out of the valve limits (Figure 3k). Taking into account the motility of the valves, the mussel viability abruptly increased at day 209 PE onwards from values below 63% to over 93% (Figure 1a).

Adjacent to the parasitized areas, the proliferative lamellae were variably fused through their extension, ranging from complete and solid fusions to partially fused lamellae (Figure 4a-f). Solid

lamellar fusions formed by hyperplastic epithelial and goblet cells, the latter mostly located at the external surface, obliterated the interlamellar spaces (Figure 4b). On the other hand, partially fused lamellae led to the occurrence of a high number of marked and well-delimited interlamellar cavities, barely visible by fresh microscopy as translucent spaces (Figure 4a). These cavities were lined by epithelial and mucus-secreting cells, contained mucinous material and cell debris, and ranged from roundish and turgid interlamellar cysts of 10–70 µm diameter to big and elongated clefts up to 150 µm length, the last opened to the exterior (Figure 4c and d). By SEM, between the fused filaments and lamellae, narrow openings were also discernible on the surface of the filamental edges, lined up by epithelial cells (Figure 4e and f).

### 3.2. The declining detachment stage (day 227–238 PE)

The parasitic loads rapidly decreased to virtually zero at day 238 PE (Figure 1b). At this stage, extensive regions of the holobranchs continued to exhibit partially fused and disordered lamellae by stereomicroscopy (Figure 5a). Histologically, half of the infested fish progressively reduced the severity and extension of their lesions displaying a less severe proliferative branchitis than that described during the rising detachment stage, with slightly hyperplastic and elongated lamellae, with their tips bent inwards (Figure 5b and c) and partially fused (Figure 5d and e). Such partially fused lamellae were accompanied by a high number of interlamellar cavities, mostly elongated clefts with abundant goblet cells arranged with their openings towards the epithelial surface (Figure 5e). On the other hand, solid lamellar fusions were less frequent in comparison to the previous stage, being restricted to well-localized areas that protruded over the filamental limits. In addition, the mixed inflammatory infiltrates related to the interlamellar system remained virtually unchanged (Figure 5c).

Related to the hypertrophied and hyperplastic lamellar fusions, certain areas revealed marked intercellular spaces and epithelial apoptosis, the latter detected by the presence of abundant shrunken cells and apoptotic bodies (Figure 5f-h). Meanwhile the number of lymphocytes decreased markedly being only observed at the base of the affected lamellae (Figure 5f), abundant phagocytic cells were intimately associated to a localized epithelial apoptosis, identified by their large cytoplasm containing eosinophilic and PAS-positive vacuoles (Figure 5g and h). Moreover, at the outermost layers, profuse shedding and degenerating pavement cells were depicted by the loss of adherence with neighboring cells, pyknosis, and swollen and vacuolized cytoplasm (Figure 5g).

### 3.3. The post-detachment stage (day 239–246 PE)

At this stage, parasitic cysts were absent (Figure 1b) and a quick and progressive regression of the previous lesions could be observed, leading to the observation of normal filamental and

lamellar architecture in the infested fish group, resembling that of the control fish (Figure 5i-k). Only mild and sporadic deviation of the filamental tips were detected, accompanied of subtle histological changes, which consisted of mild lamellar elongations and bends, a rare mild hyperplasia of the lining epithelium and a moderate number of mononuclear cells remained restricted to the lumen of the interlamellar system (Figure 5k).

## 4 DISCUSSION

The gill morphological changes observed throughout late glochidiosis of *S. salar* were related to the larval detachment of *M. margaritifera* and the subsequent recovery process, providing valuable information to understand the mechanisms involved in the larval detachment and the gill response. Hence, this study entails an exhaustive example of how the morphopathological examination of fish gills during glochidiosis may serve as an essential monitor tool to preserve fish welfare during the captive breeding programmes of endangered freshwater mussel.

During the late stages of this long-lasting parasitosis, no detrimental effects on the fish survival and body condition were observed, demonstrated by the absence of mortalities and the lack of relationship between the parasitic loads and the host fitness variables, such as the condition factor and the opercular movements. These evidences support previous observations during *M. margaritifera* glochidiosis in which sublethal parasitic loads up to 300 larvae/fish g do not have a detrimental effect on fish survival (Chowdhury *et al.*, 2019; Cunjak & McGladdery, 1991; Taeubert & Geist, 2013) neither fish body condition (Treasurer, Hastie, Hunter, Duncan & Treasurer, 2006). However, recent studies measuring the individual fish growth during a specific period described a delayed growth on fish parasitized by *M. laevis* and *M. margaritifera* (Chowdhury *et al.*, 2019; Ooue, Terui, Urabe & Nakamura, 2017). Regarding the opercular rates, no significant differences between control and exposed groups were observed and the correlation analysis between the parasitic load and the opercular rate did not showed any relationship. Nevertheless, the high mean opercular rate observed in both fish groups, 2.7 times higher than the basal rates of Atlantic salmon fry, could be explained by the stressful procedure of hand-netting (Hawkins, Armstrong & Magurran, 2004). This contrast with other authors in which *S. trutta* and *Micropterus salmoides* affected by glochidiosis showed—at resting conditions—a mild increase of the opercular rates around 1.2-1.5 times in comparison with control fish (Kaiser, 2005; Thomas *et al.*, 2013).

During fish necropsy, stereomicroscopy revealed an extremely variable outcome of glochidiosis in *S. salar*, in which exclusively one out of four lately infested salmon remained highly parasitized with 102 larvae/fish g. These differences between fish of the same experiment suggest the involvement of an individual variability, rather than being restricted to the host species

level (Taeubert, Denic, Gum, Lange & Geist, 2010; Wacker, Larsen, Karlsson & Hindar, 2019). To deal with the high parasitic load variabilities, further procedures should increase the sample size employing less-invasive methodologies. In this sense, the stereomicroscopical visualization of immersed gill tissue reveals as a potential diagnostic tool to determine *in vivo* the larval load. In comparison with a previous technique (Österling, 2011), the immersed technique enhances the stereomicroscopical visualization of parasites among filaments, avoids the introduction of instruments into the gill and exposes different holobranches and gill regions. To implement this technique, future studies need to consider the shift on the parasites distribution over the gill from a random distribution during early glochidiosis (Castrillo *et al.*, 2020) towards the focal distribution in dorsal and ventral gill areas observed in this study during the late glochidiosis. This aggregation could be influenced by the heterogeneous flow in the dorso-ventral axis (Strother, 2013) and the unidirectional water flow through the hemibranchs (Hughes, 1984), creating more sheltered regions to the water current as described in other gill ectoparasites (Kumar, Madhavi & Sailaja, 2017; Wootten, 1974).

The histopathological evaluation during the rising detachment stage (day 203–226 PE) highlighted the involvement of a proliferative branchitis surround the persistent larvae, similar to that described during early glochidiosis (Castrillo *et al.*, 2020), regarded as a common and unspecific against multiple pathogens of the salmonid gills (Tubbs, Wybourne & Lumsden, 2010). The hypertrophied and hyperplastic epithelial cells may establish long-lasting lamellar fusions playing an important role in the maintenance of the cyst covering and growth of the larvae. Such increase in size might exert pressure and tensional forces on the fused epithelium and could explain the elongation of the fused lamellae, already described during the *M. falcata* glochidiosis (Karna & Millemann, 1978).

In addition to the proliferative lesions, an inflammatory gill response was associated to the larvae, although it seems inefficient to prevent the larval encystment and development of *M. margaritifera*. In particular, the lymphocytic infiltrates observed in this study were similar to those observed around persistent glochidia at early stages (Castrillo *et al.*, 2020). In addition, deeper inflammatory infiltrates, located at the interlamellar system, may also indicate a leukocytic migration through the sinusoidal vessels, described as a defensive mechanism against bacterial and parasitic gill diseases (Adams & Nowak, 2001; Grizzle & Kiryu, 1993). Due this marked proliferative gill response, although inefficient to reject the mussel larvae, a tolerance defense strategy (Medzhitov, Schneider & Soares, 2012) should be further considered in those fish which remained highly parasitized at late stages of glochidiosis, as has been suggested in *M. margaritifera* (Barnhart et al., 2008; Marwaha et al., 2019). Other co-evolved parasitosis showed an increased tolerance response in its wild host, *S. trutta*, in contrast with the non-native host *O.*

*mykiss* (Bailey, Strepparava, Wahli & Segner, 2019), however, the understanding of the fish immune response and the tolerance/resistance mechanisms in glochidiosis deserve further study.

Although the kinetics of larval detachment cannot be fully appreciated by the techniques employed, the evaluation of the fish gill lesions throughout the rising detachment stage allowed to infer a disjoining sequence, termed as *droplet detachment*, due to the similarities with the protruding, pinch-off and detachment of a droplet fluid (Henderson, Pritchard & Smolka, 1997). Initially, the larval protrusion was observed by the apical displacement of the cyst and peduncle formation, potentially aided by the ventilatory forces in the gill chamber *e.g.*, the water flow and the abduction and adduction of the holobranchs (Strother, 2013). Pedunculated cysts were covered by a thin layer of epithelial cells which suffered mild degeneration already described by Scharsack (1994), which could be attributed to the tensional forces due the growing larvae and the water forces suffered at the outermost layers. Progressively, peduncles became constricted leading to the pinch-off of the larvae surrounded by a thin layer of epithelial cells, with no signs of "opening up" as previously described by SEM studies (Scharsack, 1994; Wächtler, Dreher-Mansur & Richter, 2001). This droplet detachment mechanism, in absence of tissue disruption, contrasted with the epithelial erosions involved in the early detachment of immature larvae in *S. salar* and *Oncorhynchus mykiss* (Castrillo *et al.*, 2020; Scharsack, 1994), suggesting a different pathogenesis between the early rejection of immature larvae and the late detachment of viable juveniles.

Meanwhile, the goblet cell hyperplasia seemed to be a chronic response in glochidiosis (Treasurer & Turnbull, 2000), not detected at earlier stages (Thomas *et al.*, 2013). This hyperplasia is particularly noticeable around constricted peduncles during the larval detachment and might contribute, by mucus secretion, to create a physical and biochemical barrier to preserve epithelial integrity at these detachment areas. In addition, the maintenance of the epithelial continuity and the goblet cell hyperplasia would prevent the occurrence of secondary infections (Dang, Pittman, Sonne, Hansson, Bach *et al.*, 2020; Karna & Millemann, 1978) and the onset of an osmoregulatory compromise, the latter observed during the epithelial erosion caused by the detachment of mature trophonts of both marine and freshwater ciliated protozoa (Colorni & Burgess, 1997; Ewing & Kocan, 1987; Tumbol *et al.*, 2001).

After the seven-months parasitism and the increase in water temperature, the larvae of *M. margaritifera* accomplished their metamorphosis, confirmed by collection of viable juveniles since day 209 PE onwards. Nevertheless, it remains unknown if temperature acts over the gill response, the juvenile development or both. The observation of the completely closed valves in the gills and the marked shift on the juvenile viability prior the detachment peak suggest an active role of the parasite during the droplet detachment, where the larval movements of the foot inside

the pallial cavity could provoke an internal motion as previously hypothesized (Kaiser, 2005; Waller & Mitchell, 1989).

Once the inciting cause was removed by the larval droplet detachment, salmon gills recovered almost completely from the parasitism of *M. margaritifera* in ~19 days after the detachment peak. This study provides shreds of evidence of a quicker gill recovery than described in glochidiosis with *Lampsilis reeviana* (Kaiser, 2005). In this case more severe lesions were attributed to a larval "excystment", whereas in *M. margaritifera* the non-erosive detachment preserved the basal membranes unaltered, essential for safeguarding the gill repair mechanisms (Kudo & Kimura, 1983; Sales *et al.*, 2017; Speare *et al.*, 1999). In addition, the high temperature maintained during this trial is expected to increase the reparative mechanisms as occurring during wound healing (Jensen, Wahli, McGurk, Eriksen, Obach *et al.*, 2015; Schmidt, 2013).

During the declining detachment stage, gill remodeling was the most important phase of the healing cascade observed in this study (Sveen, Karlsen & Ytteborg, 2020). In particular, apoptosis, phagocytosis and epithelial shedding mutually interplay to remove the cell excess, limit the detrimental effects of inflammation (AnvariFar, Amirkolaie, Miandare, Ouraji, Jalali *et al.*, 2017) and preserve the branchial architecture during healing (Daoust & Ferguson, 1986). The presence of apoptotic hallmarks related to the more constricted peduncles and the remaining lesions after the detachment peak may indicate a regression of the hyperplastic tissue, as it was suggested during other gill proliferative diseases (Sales *et al.*, 2017; Speare *et al.*, 1999) and reversible gill remodeling (Gilmour & Perry, 2018; Sollid, De Angelis, Gundersen & Nilsson, 2003). On the contrary, the absence of apoptosis during the parasitism could be explained as a beneficial mechanism both to the parasite by preserving the hyperplastic covering around the larvae (Bienvenu, Gonzalez-Rey & Picot, 2010) and also to the host by minimizing the gill surface area exposed to the external environment (Nilsson, 2007). In addition to this, the epithelial exfoliation could be involved in the removal of the outermost dying cells, as described also during the recovery of bacterial gill disease (Kudo & Kimura, 1983); providing evidence of how individualized cells slough rather than large intercellular masses (Nilsson, 2007). Due to the co-occurrence of mitosis, apoptosis and cell shedding, further quantitative studies are needed over time to provide insight about their mutual interplay during the mechanisms of gill remodeling.

During the reorganization of gill epithelium, the shift of the goblet cell distribution towards an interlamellar position points to the involvement of this cell type in the gill remodeling (Kudo & Kimura, 1983; Mueller, Sanchez, Bergman, McDonald, Rhem *et al.*, 1991). In particular, the epithelial polarization, observed by the arrangement of goblet cells towards the abundant interlamellar cavities, may help to rearrange the intercellular junctions towards the typical basolateral position (Ronza, Villamarín, Méndez, Pardo, Bermúdez *et al.*, 2019), and cleaving of

fused lamellae, as occurring during the epithelial reshaping processes (Takeichi, 2014). Interlamellar cavities are regarded as advanced lamellar fusions during glochidiosis (Castrillo *et al.*, 2020; Treasurer & Turnbull, 2000). In the absence of a mucociliary apparatus, these interlamellar cavities and the superficial openings might play an important role during the gill clearance and remodeling, allowing the hydraulic forces to act between lamellae, as it had been suggested during amoebic and bacterial gill diseases (Adams & Nowak, 2001; Speare, Ferguson, Beamish, Yager & Yamashiro, 1991).

As a result, mild sequelae were observed at the end of this experimental parasitosis, in which the filamental tip deviation could slightly perturb the hydrodynamics through gills. Moreover, the mild presence of a mixed inflammatory infiltrates at the secondary arterio-venous system should be further studied in relation with the inflammation and healing of the gills, as this vasculature might be involved in the leucocyte mobilization by removing the interstitial fluid, waste products and cellular debris; supporting further similarities with the lymphoid system of higher vertebrates (Olson, 2002; Rummer, Wang, Steffensen & Randall, 2014).

In summary, the multifocal proliferative branchitis, the non-erosive droplet detachment of the mussel juveniles and the quick and effective gill recovery suggests that experimental late glochidiosis did not severely harm fish health, supported by the absence of fish mortalities and clinical signs. This unique host-parasite interaction supposes a model to understand the role of the proliferative and remodeling epithelial responses during the defense and healing mechanisms of the gill. Moreover, the morphological techniques employed are revealed as a valuable tool during the conservation aquaculture of endangered freshwater mussels to optimize the artificial breeding programmes and evaluate the fish welfare.



## References

Adams, M. B. & Nowak, B. F. (2001). Distribution and structure of lesions in the gills of Atlantic salmon, *Salmo salar* L., affected with amoebic gill disease. *Journal of Fish Diseases, 24*(9), 535-542. doi: 10.1046/j.1365-2761.2001.00330.x

AnvariFar, H., Amirkolaie, A. K., Miandare, H. K., Ouraji, H., Jalali, M. A. & Üçüncü, S. İ. (2017). Apoptosis in fish: environmental factors and programmed cell death. *Cell and tissue research, 368*(3), 425-439. doi: 10.1007/s00441-016-2548-x

Bailey, C., Strepparava, N., Wahli, T. & Segner, H. (2019). Exploring the immune response, tolerance and resistance in proliferative kidney disease of salmonids. *Developmental & Comparative Immunology, 90*, 165-175. doi: 10.1016/j.dci.2018.09.015

Barnhart, M. C., Haag, W. R. & Roston, W. N. (2008). Adaptations to host infection and larval parasitism in Unionoida. *Journal of the North American Benthological Society, 27*(2), 370-394. doi: 10.1899/07-093.1

Bienvenu, A.-L., Gonzalez-Rey, E. & Picot, S. (2010). Apoptosis induced by parasitic diseases. *Parasites & Vectors, 3*(1), 106. doi: 10.1186/1756-3305-3-106

Castrillo, P. A., Varela-Dopico, C., Ondina, P., Quiroga, M. I. & Bermúdez, R. (2020). Early stages of *Margaritifera margaritifera* glochidiosis in Atlantic salmon: Morphopathological characterization. *Journal of Fish Diseases, 43*(1), 69-80. doi: 10.1111/jfd.13100

Chowdhury, M. M. R., Marjomäki, T. J. & Taskinen, J. (2019). Effect of glochidia infection on growth of fish: freshwater pearl mussel *Margaritifera margaritifera* and brown trout *Salmo trutta*. *Hydrobiologia*. doi: 10.1007/s10750-019-03994-4

Colorni, A. & Burgess, P. (1997). *Cryptocaryon irritans* Brown 1951, the cause of 'white spot disease' in marine fish: an update. *Aquarium Sciences and Conservation, 1*(4), 217-238. doi: 10.1023/A:1018360323287

Cunjak, R. A. & McGladdery, S. E. (1991). The parasite–host relationship of glochidia (Mollusca: Margaritiferidae) on the gills of young-of-the-year Atlantic salmon (*Salmo salar*). *Canadian Journal of Zoology, 69*(2), 353-358. doi: 10.1139/z91-055

Cuttelod, A., Seddon, M. & Neubert, E. (2011). *European red list of non-marine molluscs*: Publications office of the European Union Luxembourg.

Dang, M., Pittman, K., Sonne, C., Hansson, S., Bach, L., Søndergaard, J., Stride, M. & Nowak, B. (2020). Histological mucous cell quantification and mucosal mapping reveal different aspects of mucous cell responses in gills and skin of shorthorn sculpins (*Myoxocephalus scorpius*). *Fish & Shellfish Immunology, 100*, 334-344. doi: 10.1016/j.fsi.2020.03.020

Daoust, P. Y. & Ferguson, H. W. (1986). Potential for recovery in nodular gill disease of rainbow trout, *Salmo gairdneri* Richardson. *Journal of Fish Diseases, 9*(4), 313-318. doi: 10.1111/j.1365-2761.1986.tb01020.x

Denic, M., Taeubert, J. E. & Geist, J. (2015). Trophic relationships between the larvae of two freshwater mussels and their fish hosts. *Invertebrate Biology, 134*(2), 129-135. doi: 10.1111/ivb.12080

Ewing, M. S. & Kocan, K. M. (1987). *Ichthyophthirius multifiliis* (Ciliophora) Exit from Gill Epithelium. *Journal of Protozoology, 34*(3), 309-312. doi: 10.1111/j.1550-7408.1987.tb03181.x

Filipsson, K., Brijs, J., Näslund, J., Wengström, N., Adamsson, M., Závorka, L., Österling, E. M. & Höjesjö, J. (2017). Encystment of parasitic freshwater pearl mussel (*Margaritifera margaritifera*) larvae coincides with increased metabolic rate and haematocrit in juvenile brown trout (*Salmo trutta*). *Parasitology Research, 116*(4), 1353–1360. doi: 10.1007/s00436-017-5413-2

Geist, J. (2010). Strategies for the conservation of endangered freshwater pearl mussels *(Margaritifera margaritifera,* L.): a synthesis of Conservation Genetics and Ecology. *Hydrobiologia, 644*(1), 69-88. doi: 10.1007/s10750-010-0190-2

Gilmour, K. M. & Perry, S. F. (2018). Conflict and Compromise: Using Reversible Remodeling to Manage Competing Physiological Demands at the Fish Gill. *Physiology, 33*(6), 412-422. doi: 10.1152/physiol.00031.2018

Grizzle, J. M. & Kiryu, Y. (1993). Histopathology of Gill, Liver, and Pancreas, and Serum Enzyme Levels of Channel Catfish Infected with *Aeromonas hydrophila* Complex. *Journal of Aquatic Animal Health, 5*(1), 36-50. doi: 10.1577/1548-8667(1993)005<0036:HOGLAP>2.3.CO;2

Gum, B., Lange, M. & Geist, J. (2011). A critical reflection on the success of rearing and culturing juvenile freshwater mussels with a focus on the endangered freshwater pearl mussel (*Margaritifera margaritifera* L.). *Aquatic Conservation: Marine and Freshwater Ecosystems, 21*(7), 743-751. doi: 10.1002/aqc.1222

Hawkins, L. A., Armstrong, J. D. & Magurran, A. E. (2004). Predator-induced hyperventilation in wild and hatchery Atlantic salmon fry. *Journal of Fish Biology, 65*(s1), 88-100. doi: https://doi.org/10.1111/j.0022-1112.2004.00543.x

Henderson, D. M., Pritchard, W. G. & Smolka, L. B. (1997). On the pinch-off of a pendant drop of viscous fluid. *Physics of Fluids, 9*(11), 3188-3200. doi: 10.1063/1.869435

Hruska, J. (1992). The freshwater pearl mussel in South Bohemia: evaluation of the effect of temperature on reproduction, growth and age structure of the population. *Archiv Fur Hydrobiologie, 126*(2), 181-191.

Hughes, G. M. (1984). General Anatomy of the Gills. *Fish Physiology, Volume 10, Part A*, 1-72. doi: 10.1016/S1546-5098(08)60317-9

Jensen, L. B., Wahli, T., McGurk, C., Eriksen, T. B., Obach, A., Waagbø, R., Handler, A. & Tafalla, C. (2015). Effect of temperature and diet on wound healing in Atlantic salmon (*Salmo salar* L.). *Fish Physiology and Biochemistry, 41*(6), 1527-1543. doi: 10.1007/s10695-015-0105-2

Kaiser, B. E. (2005). *The effects of glochidiosis on fish respiration.* (Doctoral dissertation, Missouri State University, Springfield, Missouri). Retrieved from https://www.swan.searchmobius.org/search~S6/o66473455

Karna, D. W. & Millemann, R. E. (1978). Glochidiosis of salmonid fishes. III. Comparative susceptibility to natural infection with *Margaritifera margaritifera* (L.) (Pelecypoda: Margaritanidae) and associated histopathology. *Journal of Parasitology, 64*(3), 528-537. doi: 10.2307/3279799

Kudo, S. & Kimura, N. (1983). The Recovery from Hyperplasia in an Artificial Infection. *Bulletin of the Japanese Society of Scientific Fisheries, 49*(11), 1635-1641. doi: 10.2331/suisan.49.1635

Kumar, R., Madhavi, R. & Sailaja, B. (2017). Spatial distribution of ectoparasites on the gills of the mullet, *Liza macrolepis*: the effects of pollution. *Journal of Parasitic Diseases, 41*(1), 40-47. doi: 10.1007/s12639-015-0746-1

Lois, S., Ondina, P., Outeiro, A., Amaro, R. & San Miguel, E. (2014). The north-west of the Iberian Peninsula is crucial for conservation of *Margaritifera margaritifera* (L.) in Europe. *Aquatic Conservation: Marine and Freshwater Ecosystems, 24*(1), 35-47. doi: 10.1002/aqc.2352

Marwaha, J., Aase, H., Geist, J., Stoeckle, B. C., Kuehn, R. & Jakobsen, P. J. (2019). Host (*Salmo trutta*) age influences resistance to infestation by freshwater pearl mussel (*Margaritifera margaritifera*) glochidia. *Parasitology Research, 118*(5), 1519-1532. doi: 10.1007/s00436-019-06300-2

Medzhitov, R., Schneider, D. S. & Soares, M. P. (2012). Disease Tolerance as a Defense Strategy. *Science, 335*(6071), 936-941. doi: 10.1126/science.1214935

Mueller, M. E., Sanchez, D. A., Bergman, H. L., McDonald, D. G., Rhem, R. G. & Wood, C. M. (1991). Nature and Time Course of Acclimation to Aluminum in Juvenile Brook Trout (*Salvelinus fontinalis*). II. Gill Histology. *Canadian Journal of Fisheries and Aquatic Sciences, 48*(10), 2016-2027. doi: 10.1139/f91-240

Nilsson, G. E. (2007). Gill remodeling in fish–a new fashion or an ancient secret? *Journal of Experimental Biology, 210*(14), 2403-2409. doi: 10.1242/jeb.000281

Olson, K. R. (2002). Vascular anatomy of the fish gill. *Journal of Experimental Zoology, 293*(3), 214-231. doi: 10.1002/jez.10131

Ooue, K., Terui, A., Urabe, H. & Nakamura, F. (2017). A delayed effect of the aquatic parasite *Margaritifera laevis* on the growth of the salmonid host fish *Oncorhynchus masou masou*. *Limnology, 18*(3), 345-351. doi: 10.1007/s10201-017-0514-2

Österling, M. E. (2011). Test and application of a non-destructive photo-method investigating the parasitic stage of the threatened mussel *Margaritifera margaritifera* on its host fish *Salmo trutta*. *Biological Conservation, 144*(12), 2984-2990. doi: 10.1016/j.biocon.2011.09.001

Österling, M. E., Ferm, J. & Piccolo, J. J. (2014). Parasitic freshwater pearl mussel larvae (*Margaritifera margaritifera* L.) reduce the drift-feeding rate of juvenile brown trout (*Salmo trutta* L.). *Environmental Biology of Fishes, 97*(5), 543-549. doi: 10.1007/s10641-014-0251-x

Powell, M. D., Leef, M. J., Roberts, S. D. & Jones, M. A. (2008). Neoparamoebic gill infections: Host response and physiology in salmonids. *Journal of Fish Biology, 73*(9), 2161-2183. doi: 10.1111/j.1095-8649.2008.02053.x

Preston, S. J., Keys, A. & Roberts, D. (2007). Culturing freshwater pearl mussel *Margaritifera margaritifera*: a breakthrough in the conservation of an endangered species. *Aquatic Conservation: Marine and Freshwater Ecosystems, 17*(5), 539-549. doi: 10.1002/aqc.799

R Core Team. (2019). R: a language and environment for statistical computing: R Foundation for Statistical Computing, Vienna, Austria. Retrieved from https://www.R-project.org/

Ronza, P., Villamarín, A., Méndez, L., Pardo, B. G., Bermúdez, R. & Quiroga, M. I. (2019). Immunohistochemical expression of E–cadherin in different tissues of the teleost fish *Scophthalmus maximus*. *Aquaculture, 501*, 465-472. doi: 10.1016/j.aquaculture.2018.12.009

Rummer, J. L., Wang, S., Steffensen, J. F. & Randall, D. J. (2014). Function and control of the fish secondary vascular system, a contrast to mammalian lymphatic systems. *The Journal of experimental biology, 217*(5), 751-757. doi: 10.1242/jeb.086348

Sales, C. F., Santos, K. P. E. d., Rizzo, E., Ribeiro, R. I. M. d. A., Santos, H. B. d. & Thomé, R. G. (2017). Proliferation, survival and cell death in fish gills remodeling: From injury to recovery. *Fish & Shellfish Immunology, 68*, 10-18. doi: 10.1016/j.fsi.2017.07.001

Scharsack, G. (1994). *Licht- und elektronenmikroskopische Untersuchungen an Larvalstadien einheimischer Unionacea (Bivalvia; Eulamellibranchiata) [Light and electron microscopic studies on larval stages of native Unionacea (Bivalvia, Eulamellibranchiata)].* (Unpublished doctoral dissertation), Universität Hannover, Hannover, Germany. Retrieved from http://www.repo.uni-hannover.de/handle/123456789/5643

Schmidt, J. G. (2013). *Wound healing in rainbow trout (Oncorhynchus mykiss) and common carp (Cyprinus carpio) with a focus on gene expression and wound imaging.* Technical University of Denmark.

Sollid, J., De Angelis, P., Gundersen, K. & Nilsson, G. E. (2003). Hypoxia induces adaptive and reversible gross morphological changes in crucian carp gills. *Journal of Experimental Biology, 206*, 3667-3673. doi: 10.1242/jeb.00594

Speare, D. J., Carvajal, V. & Horney, B. S. (1999). Growth Suppression and Branchitis in Trout Exposed to Hydrogen Peroxide. *Journal of Comparative Pathology, 120*(4), 391-402. doi: 10.1053/jcpa.1998.0285

Speare, D. J., Ferguson, H. W., Beamish, F. W. M., Yager, J. A. & Yamashiro, S. (1991). Pathology of bacterial gill disease: ultrastructure of branchial lesions. *Journal of Fish Diseases, 14*(1), 1-20. doi: 10.1111/j.1365-2761.1991.tb00572.x

Strother, J. A. (2013). Hydrodynamic resistance and flow patterns in the gills of a tilapine fish. *The Journal of experimental biology, 216*(14), 2595. doi: 10.1242/jeb.079517

Sveen, L., Karlsen, C. & Ytteborg, E. (2020). Mechanical induced wounds in fish – a review on models and healing mechanisms. *Reviews in Aquaculture, n/a*(n/a). doi: 10.1111/raq.12443

Taeubert, J. E., Denic, M., Gum, B., Lange, M. & Geist, J. (2010). Suitability of different salmonid strains as hosts for the endangered freshwater pearl mussel (*Margaritifera margaritifera* L.). *Aquatic Conservation: Marine and Freshwater Ecosystems, 20*(7), 728-734. doi: 10.1002/aqc.1147

Taeubert, J. E. & Geist, J. (2013). Critical swimming speed of brown trout (*Salmo trutta*) infested with freshwater pearl mussel (*Margaritifera margaritifera*) glochidia and implications for artificial breeding of an endangered mussel species. *Parasitology Research, 112*(4), 1607-1613. doi: 10.1007/s00436-013-3314-6

Taeubert, J. E., Gum, B. & Geist, J. (2013). Variable development and excystment of freshwater pearl mussel (*Margaritifera margaritifera* L.) at constant temperature. *Limnologica - Ecology and Management of Inland Waters, 43*(4), 319-322. doi: 10.1016/j.limno.2013.01.002

Takeichi, M. (2014). Dynamic contacts: rearranging adherens junctions to drive epithelial remodelling. *Nature Reviews Molecular Cell Biology, 15*(6), 397-410. doi: 10.1038/nrm3802

Thomas, G. R., Taylor, J. & Garcia de Leaniz, C. (2013). Does the parasitic freshwater pearl mussel *M. margaritifera* harm its host? *Hydrobiologia, 735*(1), 191-201. doi: 10.1007/s10750-013-1515-8

Treasurer, J. W., Hastie, L. C., Hunter, D., Duncan, F. & Treasurer, C. M. (2006). Effects of (*Margaritifera margaritifera*) glochidial infection on performance of tank-reared Atlantic salmon (*Salmo salar*). *Aquaculture, 256*(1–4), 74-79. doi: 10.1016/j.aquaculture.2006.02.031

Treasurer, J. W. & Turnbull, T. (2000). The pathology and seawater performance of farmed Atlantic salmon infected with glochidia of *Margaritifera margaritifera*. *Journal of Fish Biology, 57*(4), 858-866. doi: 10.1111/j.1095-8649.2000.tb02197.x

Tubbs, L., Wybourne, B. A. & Lumsden, J. S. (2010). Nodular gill disease causing proliferative branchitis and mortality in Chinook salmon (*Oncorhynchus tshawytscha*). *N Z Vet J, 58*(1), 59-61. doi: 10.1080/00480169.2010.65061

Tumbol, R. A., Powell, M. D. & Nowak, B. F. (2001). Ionic Effects of Infection of *Ichthyophthirius multifiliis* in Goldfish. *Journal of Aquatic Animal Health, 13*(1), 20-26. doi: 10.1577/1548-8667(2001)013<0020:IEOIOI>2.0.CO;2

Vaughn, C. C. (2017). Ecosystem services provided by freshwater mussels. *Hydrobiologia, 810*(1), 15-27. doi: 10.1007/s10750-017-3139-x

Wächtler, K., Dreher-Mansur, M. & Richter, T. (2001). Larval Types and Early Postlarval Biology in Naiads (Unionoida). In G. Bauer & K. Wächtler (Eds.), *Ecology and Evolution of the Freshwater Mussels Unionoida* (Vol. 145, pp. 93-125): Springer Berlin Heidelberg.

Wacker, S., Larsen, B. M., Karlsson, S. & Hindar, K. (2019). Host specificity drives genetic structure in a freshwater mussel. *Scientific Reports, 9*(1), 10409. doi: 10.1038/s41598-019-46802-8

Waller, D. L. & Mitchell, L. G. (1989). Gill tissue reactions in walleye *Stizostedion vitreum vitreum* and common carp *Cyprinus carpio* to glochidia of the freshwater mussel *Lampsilis radiata siliquoidea*. *Diseases of Aquatic Organisms, 6*(2), 81-87. doi: 10.3354/dao006081

Wootten, R. (1974). The spatial distribution of *Dactylogyrus amphibothrium* on the gills of ruffe *Gymnocephalus cernua* and its relation to the relative amounts of water passing over the parts of the gills. *Journal of Helminthology, 48*(03), 167-174. doi: 10.1017/S0022149X00022793

654 **Figures**

655 Figure 1. (a and b) Evolution of the mussel juvenile detachment (a) in relation with the fish
656 parasitosis (b) during the three stages of late glochidiosis of *M. margaritifera* delimited by dashed
657 red lines. (c) No correlation between the parasitic loads and the fish body condition nor the
658 opercular rate were detected in the correlation analysis. Individuals with parasitic loads in the
659 upper quartile were represented in red. Confidence interval was 95%.

660 Figure 2. Main morphopathological findings during the rising detachment stage of late *M.*
661 *margaritifera* glochidiosis. (a) Gill macrophotography of an infested fish with punctiform lesions
662 which corresponded with the encysted larvae (arrows). (b and c) Stereomicrophotographs
663 showing the bean-shaped larvae located between each pair of hemibranchs indicated with
664 arrowheads. (d) Distribution of parasites clustered in bunches at the dorsal and ventral regions of
665 each holobranch (asterisks). (e) The localized epithelial response enclosing the parasitic cysts was
666 accompanied by severe lamellar and filamental fusions (asterisks). Note the concave depressions
667 on the filament surface contiguous to an adjacent larva (arrows). H&E stain. (f) Surround the
668 outer surface of the parasitic cyst (arrowheads), the fused and elongated lamellae (dashed lines)
669 were related to abundant mitotic figures (circles) and interlamellar cysts (arrow). Note the
670 pleomorphic inflammatory infiltrate located at the interlamellar system (asterisks). H&E stain.
671 (g) A high number of lymphocytes interspersed between epithelial cells, the latter became
672 flattened and eosinophilic towards the larvae (arrowheads). H&E stain. Inset: The eosinophilic
673 epithelial cells (arrows) beside the parasitic cysts (arrowheads) became thinner and more intensely
674 stained under the PAS stain. (h) Interlamellar system with a pleomorphic inflammatory (asterisks)
675 underneath the intricate basement membrane highlighted with the Masson-Goldner trichrome
676 stain. (i and j) Comparison between infested fish with marginated macrophages and
677 polymorphonuclear cells over the interlamellar system endothelia (arrowheads, i) and control fish
678 showing a normal lamellar morphology without leukocytes over the endothelial cells lining the
679 interlamellar system (arrowheads, j). H&E stains.

680 Figure 3. Gill morphopathology of the most superficial parasitic cysts during the rising
681 detachment stage of late *M. margaritifera* glochidiosis (a-h) and the *droplet detachment* (i) from
682 encysted larvae into free-living juveniles (j and k). (a) Scanning electron microscopy (SEM) of a
683 cluster of buoyant encysted larvae (asterisks). (b and c) Fresh microphotographs comparing the
684 unaltered arterioles (b, arrowheads) with exceptionally devious arterioles (c, arrowheads). (d and
685 e) Deviation of the growth plaque (arrowheads, d) and a well-localized cartilage hyperplasia
686 (arrowheads, e) overgrowing over the cartilage ray (asterisk, e). H&E and Masson-Goldner
687 trichrome stain, respectively. (f) SEM of a parasitic cyst completely covered by epithelial cells
688 with the dashed area highlighting the most protruding area. Inset: Detail of the dashed area with

689 poorly discernible microridges over the epithelial surface (arrowheads). (g) Histological
690 microphotograph of the hyperplastic peduncles (asterisk) anchoring the larvae to the gill
691 filaments. Note the presence of an elongate lamella (dashed line). H&E stain. (h) Constricted
692 peduncle with a high number of goblet cells lined up the epithelial surface (asterisks) and high
693 number of apoptotic (arrowheads) and phagocytic bodies (arrows) at deeper regions. PAS stain.
694 (i) Schematic illustration of the three-steps droplet detachment of the mussel juveniles. (j) Fresh
695 light microscopy of an encysted larvae with the valve rims facing each other (arrowheads) and
696 their internal pallial cavity (asterisk). (k) Stereomicrophotograph of recently detached and viable
697 juveniles with their protractile foot (arrowheads).

698 Figure 4. Fusions and interlamellar cavities adjacent to the encysted larvae during the rising
699 detachment stage of late *M. margaritifera* glochidiosis. (a) The limits of the interlamellar cavities
700 were barely visible by fresh microscopy (arrowheads) close to the parasitic cysts (asterisks). Inset.
701 Detail of an interlamellar cyst associated with two fused lamellae (arrowheads). (b) Solid lamellar
702 fusion (dashed lines) associated with the presence of abundant interlamellar mitotic figures
703 (encircled) and goblet cells at the surface (asterisks). PAS stain. (c and d). Partially fused lamellae
704 characterized by the presence of interlamellar cysts (asterisks) and clefts (arrowheads) surrounded
705 by mucous cells. PAS stains. (e) SEM of two fused filaments (dashed line) with small openings
706 located between partially fused lamellae (arrowheads). (f) Detail of the dashed area highlighting
707 two interlamellar openings (asterisks) lined up by epithelial cells.

708 Figure 5. Gill morphopathology during the declining detachment stage (a–h) and the post-
709 detachment stage of late *M. margaritifera* glochidiosis (i–k). (a) Stereomicroscopical image of
710 disordered lamellae observed by tousled secondary filaments (arrowheads). (b) By histology,
711 altered lamellae ranged from hyperplastic and fused lamellae (asterisks) to elongated and bent
712 lamellae (arrowheads). H&E stain. (c) Detail of elongated lamellae with their tips bent inwards
713 and slightly hyperplastic (arrowheads). Note the presence of a moderate number of pleomorphic
714 inflammatory cells at the interlamellar system (asterisks). H&E stain. (d) Hyperplastic and fused
715 lamellar tips (arrowheads) giving rise to an elongated interlamellar cavity (asterisk). H&E stain.
716 (e) Detail of hyperplastic lamellae with most of the goblet cells arranged towards the interlamellar
717 clefts (arrowheads) with openings towards the surface (arrowheads). PAS stain. (f) Partially fused
718 lamellae showed areas of moderate lymphocytic (asterisks) and localized areas of epithelial
719 degeneration (arrows). H&E stain. (g) Detailed microphotograph of abundant apoptotic bodies
720 (asterisks) and vacuolized, swollen and sloughing epithelial cells at the outer surface
721 (arrowheads). H&E stain. (h) Phagocytosis of apoptotic bodies (arrowheads) and small PAS-
722 positive vacuoles (arrows) was associated with an area of lamellar fusion. PAS stain. (i and j)
723 Normal structure of outer surface of the gill by stereomicroscopy (i) and scanning electron

724 microscopy (j). (k) Histological photograph showing mild epithelial hyperplasia, elongations and
725 lamellar deviation (arrowheads) together with a moderate number of mononuclear cells at the
726 interlamellar system (asterisks). H&E stain.

727 Supplementary table and figure are included in Supporting Information.

728

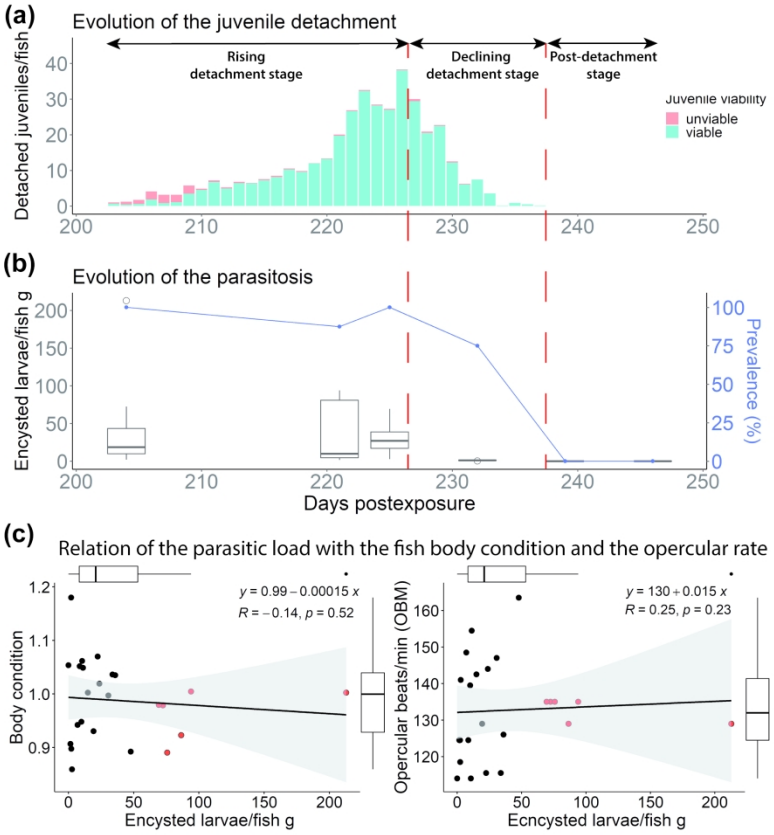
(a)
Evolution of the juvenile detachment
Rising detachment stage
Declining detachment stage
Post-detachment stage
Detached juveniles/fish
Juvenile viability
unviable
viable
(b)
Evolution of the parasitosis
Encysted larvae/fish g
Prevalence (%)
Days postexposure
(c)
Relation of the parasitic load with the fish body condition and the opercular rate
y = 0.99 − 0.00015 x
R = −0.14, p = 0.52
Body condition
Encysted larvae/fish g
y = 130 + 0.015 x
R = 0.25, p = 0.23
Opercular beats/min (OBM)
Encysted larvae/fish g

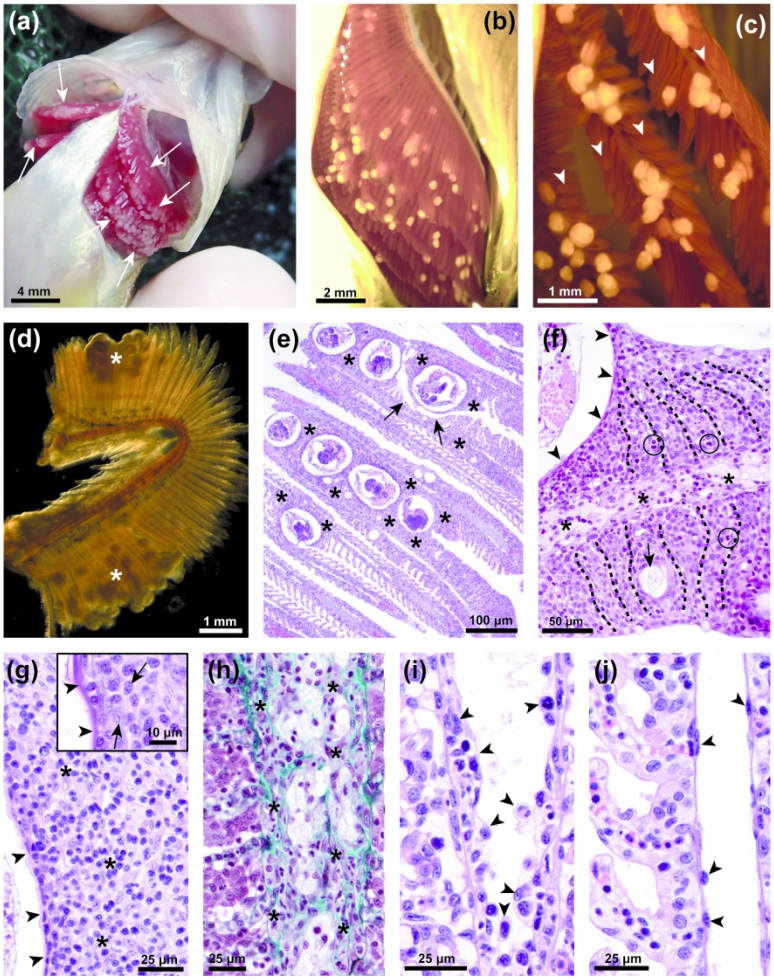
(a)
4 mm
(b)
2 mm
(c)
1 mm
(d)
1 mm
(e)
100 µm
(f)
50 µm
(g)
10 µm
25 µm
(h)
25 µm
(i)
25 µm
(j)
25 µm

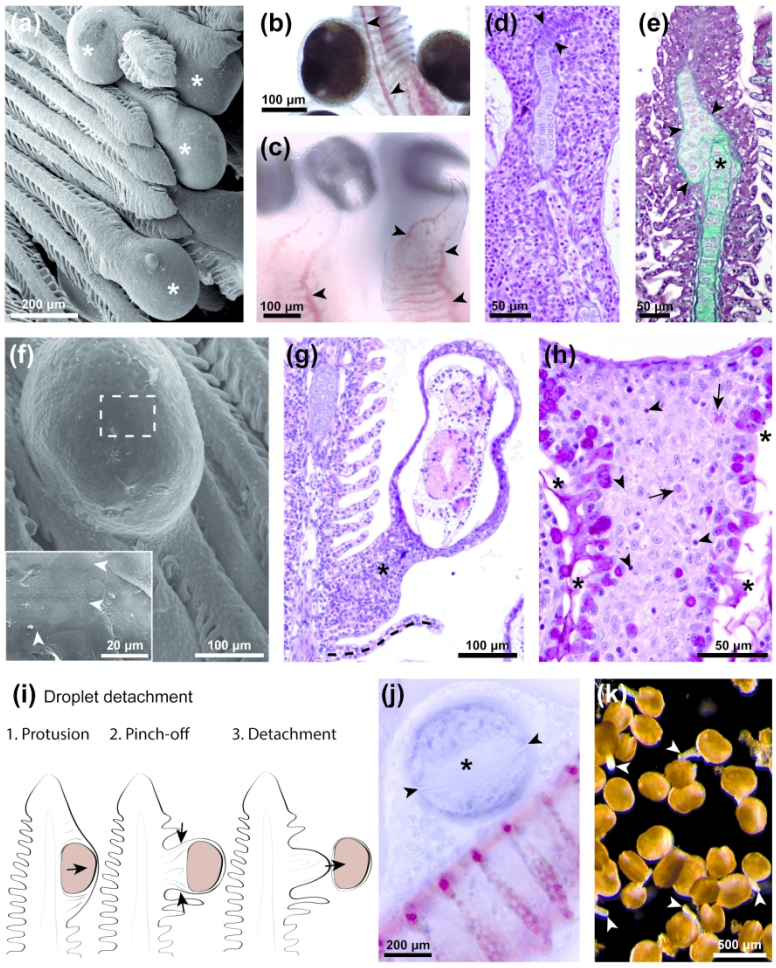
(a)
200 µm
(b)
100 µm
(c)
100 µm
(d)
50 µm
(e)
50 µm
(f)
20 µm
100 µm
(g)
100 µm
(h)
50 µm
(i) Droplet detachment
1. Protusion
2. Pinch-off
3. Detachment
(j)
200 µm
(k)
500 µm

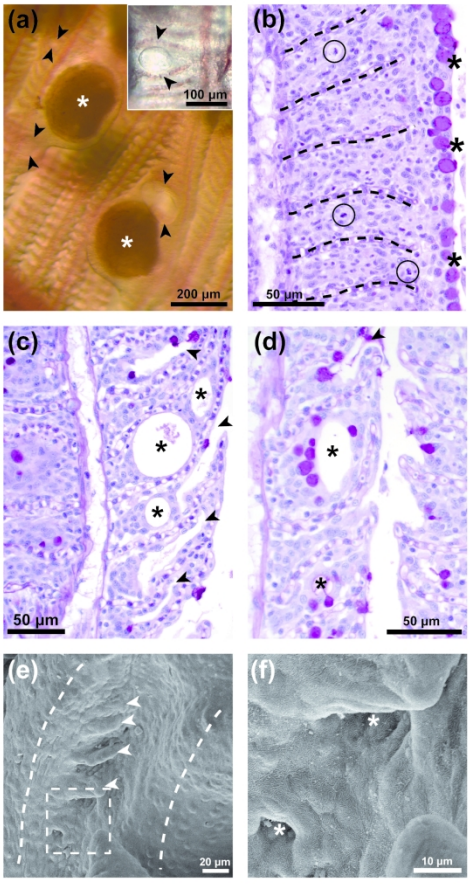
(a)
100 µm
200 µm
(b)
50 µm
(c)
50 µm
(d)
50 µm
(e)
20 µm
(f)
10 µm

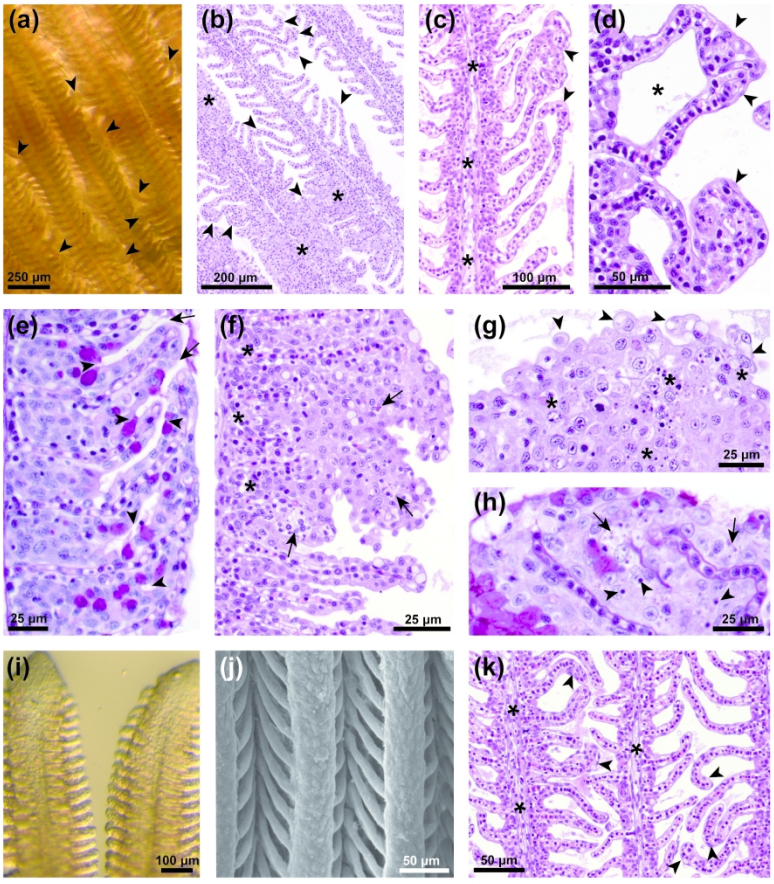
(a)
250 µm
(b)
200 µm
(c)
100 µm
(d)
50 µm
(e)
25 µm
(f)
25 µm
(g)
25 µm
(h)
25 µm
(i)
100 µm
(j)
50 µm
(k)
50 µm

**Supporting Information**

Supplementary table 1. Physico-chemical parameters of water in the control and infested fish groups between day 202 and 246 postexposure (PE) after the glochidial infestation. Nitrogen compounds are expressed in mg/L and temperature (± 0.2) is expressed in Celsius degrees (ºC).

| | | Control group | | | | | | Infested group | | | | | |
|---|---|---|---|---|---|---|---|---|---|---|---|---|---|
| Days PE | ºC | $NH^3$ & $NH^4$ | $NH^3$ | $NO^{-2}$ | $NO^{-3}$ | pH | DO (%) | $NH^3$ & $NH^4$ | $NH^3$ | $NO^{-2}$ | $NO^{-3}$ | pH | DO (%) |
| **202** | 11 | 0.14 | 0.0002 | 0.03 | 2.8 | 6.8 | 90 | 0.11 | 0.0001 | 0.04 | 1.2 | 6.8 | 86 |
| **204** | 13 | 0.15 | 0.0002 | 0.04 | 4.6 | 6.7 | 87 | 0.11 | 0.0003 | 0.02 | 5.3 | 7.0 | 90 |
| **208** | 17 | 0.16 | 0.0003 | 0.04 | 3.0 | 6.8 | 85 | 0.15 | 0.0004 | 0.04 | 4.1 | 6.9 | 84 |
| **212** | 17 | 0.08 | 0.0002 | 0.04 | 1.3 | 6.9 | 88 | 0.14 | 0.0005 | 0.05 | 1.2 | 7.0 | 91 |
| **219** | 17 | 0.09 | 0.0002 | 0.03 | 4.3 | 6.9 | 93 | 0.07 | 0.0002 | 0.05 | 2.3 | 7.0 | 93 |
| **221** | 17 | 0.14 | 0.0005 | 0.04 | 1.6 | 7.0 | 91 | 0.09 | 0.0004 | 0.04 | 0.4 | 7.1 | 86 |
| **225** | 17 | 0.18 | 0.0005 | 0.03 | 2.0 | 6.9 | 91 | 0.13 | 0.0004 | 0.05 | 3.1 | 7.0 | 90 |
| **232** | 17 | 0.20 | 0.0007 | 0.06 | 1.6 | 7.0 | 92 | 0.04 | 0.0001 | 0.05 | 3.8 | 6.9 | 88 |
| **239** | 17 | 0.15 | 0.0003 | 0.11 | 5.4 | 6.8 | 87 | 0.05 | 0.0001 | 0.03 | 3.5 | 6.9 | 87 |
| **246** | 17 | 0.10 | 0.0003 | 0.06 | 3.8 | 6.9 | 90 | 0.13 | 0.0003 | 0.04 | 3.3 | 6.8 | 91 |

Supplementary figure 1. Comparison of the evolution of the fish body condition (a) and the opercular rate after hand-netting (b) between control and infested fish groups. The asterisks (*) denote the significant differences between groups ($p$-value <0.05).